ANL-79-110

ANL-79-110

ADVANCED FUEL CELL DEVELOPMENT

Progress Report for July—September 1979

by

R. D. Pierce, K. Kinoshita, G. H. Kucera,
R. B. Poeppel, J. W. Sim, and R. N. Singh

ARGONNE NATIONAL LABORATORY

ARGONNE NATIONAL LABORATORY, ARGONNE, ILLINOIS

Prepared for the U. S. DEPARTMENT OF ENERGY
under Contract W-31-109-Eng-38

Distribution Category:
Energy Conversion
(UC-93)

ANL-79-110

ARGONNE NATIONAL LABORATORY
9700 South Cass Avenue
Argonne, Illinois 60439

ADVANCED FUEL CELL DEVELOPMENT

Progress Report for
July—September 1979

by

R. D. Pierce, K. Kinoshita, G. H. Kucera,
R. B. Poeppel*, J. W. Sim, and R. N. Singh*

Chemical Engineering Division

February 1980

Previous reports in this series

ANL-79-84	April—June 1979
ANL-79-51	January—March 1979
ANL-79-28	October—December 1978
ANL-78-95	July—September 1978

*Materials Science Division, ANL

TABLE OF CONTENTS

LIST OF FIGURES

LIST OF TABLES

CHEMICAL ENGINEERING DIVISION

ADVANCED FUEL CELL DEVELOPMENT

July—September 1979

by

R. D. Pierce, K. Kinoshita, G. H. Kucera,
R. B. Poeppel, J. W. Sim, and R. N. Singh

ABSTRACT

This report describes advanced fuel cell research and development activities at Argonne National Laboratory (ANL) during the period July—September 1979. These efforts have been directed toward understanding and improving components of the molten carbonate fuel cells operated at temperatures near 925 K.

The primary focus has been on the development of electrolyte structures that have good electrolyte retention and mechanical properties as well as long-term stability. A major effort this period has been on the synthesis of $LiAlO_2$ particles for the preparation of high-porosity (60%) sintered structures. The major problem has been avoidance of ionic species (unreacted Li_2CO_3 or LiOH) during sintering, which produce structures with excessive particle growth and low porosity. Initial cell tests with sintered electrolyte structures indicate that these structures can survive thermal cycles and that adequate wet seals can be obtained.

SUMMARY

Synthesis of $LiAlO_2$

The major effort on the synthesis of $LiAlO_2$ powders was directed to the preparation of material for sintered structures. The γ-$LiAlO_2$ powder prepared by a two-stage heat treatment (875 K and $\sim$1175 K) of γ-Al_2O_3 and Li_2CO_3 was found to be sensitive to humidity during the blending of the powders. For example, the γ-$LiAlO_2$ product had a surface area of $\sim$7 m^2/g when blended at $\sim$10% relative humidity, and $\sim$1 m^2/g when blended at $\sim$45% relative humidity. The moisture has an adverse effect on the blending of the reactants and promotes particle growth by dissolution and redeposition. The most promising approach for the fabrication of $LiAlO_2$ for sintered structures involves low-cost $Al(OH)_3$ impregnated with LiOH and fired at 725 K to produce β-$LiAlO_2$. A pellet of $\sim$60% porosity was sintered at 1175 K from some of this product; however, the products, to date, have been contaminated with γ-Al_2O_3.

Development of Sintered $LiAlO_2$ Structures

The feasibility of sintering 12.5-cm-square $LiAlO_2$ structures with and without wire reinforcement has been demonstrated. A number of sintered structures fabricated from different batches of γ-$LiAlO_2$ powder were found to have porosities ranging from 35 to 60%. Several specimens were examined by SEM to

determine the microstructural features responsible for the low-porosity levels, and a major fraction of coarse particles was thought to be responsible for lower porosity samples.

To determine the minimum suitable temperature for converting α- to γ-$LiAlO_2$, high-surface-area α-$LiAlO_2$ powders were heat-treated at 973, 1023, and 1073 K. The samples prepared at 1023 and 1073 K converted to the γ-phase, but the α-phase predominated in the samples heat treated at 973 K, even after 50 h. Sintered discs with porosities between 47 and 58% were fabricated from powder that had been transformed to γ-$LiAlO_2$ at 1023 or 1073 K. This porosity is higher than the ∿45% obtained previously when the transformation temperature was 1175 K.

Sintered structures with porosities >60% were fabricated directly from an α-$LiAlO_2$ powder. When this powder contained unreacted Li_2CO_3, the product had low porosity because of rapid particle growth. Additional sintered structures will be prepared from α-$LiAlO_2$ powders.

Examination of Electrolyte Structures

X-ray radiography on a sintered structure (6-P) that had been tested in a circular cell (Sinter 2) was performed. This structure showed good wet-seal and cross-leakage characteristics. A crack was observed which initiated at one specimen edge but did not propagate through the tile beyond the wet seal. Scanning electron micrographs were taken of crack surfaces present in another sintered electrolyte structure (1-P) that had been tested in a cell (Sinter 1) and revealed that the surface inside the wet-seal area had less electrolyte than the area outside the wet seal. A hot-pressed tile (T159-57) not tested in a cell was examined by SEM and found to have an inhomogeneous microstructure similar to that observed in the tiles examined following cell testing.

Thermomechanical Testing

The coefficient of linear thermal expansion and creep data have been determined for hot-pressed pellets consisting of high-surface-area γ-$LiAlO_2$ (26 m^2/g) and variable amounts of Li_2CO_3-K_2CO_3 eutectic. The coefficients of thermal expansion, which were determined for the temperature range from room temperature to ∿675 K, varied from $12.0 \pm 1.8 \times 10^{-6}$/°C for pellets having 6.4 vol % eutectic to $30.6 \pm 1.5 \times 10^{-6}$/°C for pellets containing 84.2 vol % eutectic. The pellet showed typical primary creep behavior at the fuel cell operating temperature (925 K), that is, the rate decreased with time.

Cell Testing

A reinforced sintered electrolyte structure that contained two very small cracks was employed in cell Sinter 3. The cell had low cross-leakage on startup, but the leakage increased significantly after the first thermal cycle to room temperature; the leakage rate showed no further change after the second cycle. Subsequently, cell operation was terminated because of carbon deposition in the anode inlet tube. It appears that any detectable cracks in the electrolyte structure will lead to cross-leakage during cell operation.

I. INTRODUCTION

The advanced fuel cell studies at Argonne National Laboratory (ANL) are part of the DOE Second Generation Fuel Cell Program. The goal of this DOE program is the earliest possible introduction of high-efficiency generating systems based on molten-carbonate fuel cells, which have the capability of operating on coal or other fuels. At the present stage of development, the primary thrust of the ANL program is directed to development of the fuel cell itself.

A molten carbonate fuel cell consists of a porous nickel anode, a porous nickel oxide cathode, an electrolyte structure which separates the anode and cathode and conducts only ionic current between them, and appropriate metal housings or, in the case of stacks of cells, intercell separator sheets. The cell housings (or separator sheets) bear upon the electrolyte structure to form a seal between the environment and the anode and cathode gas compartments. The electrolyte structure, which is commonly called "tile", is usually a composite structure of discrete $LiAlO_2$ particles and a mixture of alkali metal carbonates, which are liquid at the cell operating temperature of 925 K. At the anode, hydrogen and carbon monoxide in the fuel gas react with carbonate ion from the electrolyte to form carbon dioxide and water, while giving up electrons to the external circuit. At the cathode, carbon dioxide and oxygen react and accept electrons from the external circuit to re-form carbonate ion, which is conducted through the electrolyte to the anode. In a practical cell stack, CO_2 from the cathode probably would be obtained from the anode exhaust.

The ANL contribution to the program is intended to provide understanding of cell behavior and to develop improved components and processes. Improvements are needed in the electrolyte structure, which is receiving special attention at ANL. Characterization of tile properties and the relation of the properties to tile behavior in cells is of major importance. Determination of the stability of tile materials is also of high priority. The present electrolyte structure generally is a clay-like mixture of fine $LiAlO_2$ particles and carbonate salt; however, structures employing a sintered $LiAlO_2$ matrix also are being examined.

Operation of cells is required for assessment of the behavior of the electrolyte and other components and for understanding of the performance and life-limiting mechanisms at work within the cell. Cell operation is, of course, coupled with a diagnostic effort and a materials-development effort.

II. SYNTHESIS OF LITHIUM ALUMINATE
(K. Kinoshita and J. W. Sim)

An objective of the electrolyte development effort at ANL is to develop methods to synthesize $LiAlO_2$ electrolyte structures for cell testing and to develop methods to produce low-cost electrolyte structures sufficiently stable for use in molten carbonate fuel cells.

Previous results (ANL-78-40, p. 7) showed that high-surface-area γ-$LiAlO_2$ ($\geq$20 m /g) for paste electrolyte structures (tiles) can be obtained by the two-stage heat treatment (775 K for 2 h followed by 975 K for 16 h) of physical mixtures of LiOH, γ-Al_2O_3 (Degussa) and the appropriate amount of Li_2CO_3 and K_2CO_3 for the electrolyte phase. This γ-$LiAlO_2$ also would appear to be desirable for use in sintered structures, but the carbonate phase must be removed first. Therefore, we have employed other synthesis procedures in an attempt to produce $LiAlO_2$ free of carbonates. Since the start of 1979, several batches of γ-$LiAlO_2$ have been prepared for use in sintered structures by heat treatment (875 K then $\sim$1175 K) of physical mixtures of γ-Al_2O_3 (Degussa) and Li_2CO_3. Table 1 summarizes these runs, which are listed in chronological order.

Some difficulties were encountered in achieving high porosities ($\sim$60%) in the sintered structures prepared from some of these batches of γ-$LiAlO_2$; therefore, we reviewed the synthesis procedure to determine the nature and cause of the differences among the batches. Samples 134-82 and 134-83 were prepared from Li_2CO_3 and γ-Al_2O_3 that were physically mixed in a plastic jar containing two rubber stoppers instead of the two alumina balls used in previous samples. This slight variation in the mixing procedure produced a powder of higher bulk density and could account for the low surface area of the γ-$LiAlO_2$ (0.4 m^2/g). It was apparent from subsequent samples that other factors also affected the surface area of the final product. According to the data in Table 1, the surface area of γ-$LiAlO_2$ powders prepared in the winter months, when the relative humidity in the laboratory was low ($\sim$10%), had the highest surface area (6-7.6 m^2/g); whereas, in other months, when the relative humidity was high (40-50%), the surface area of the γ-$LiAlO_2$ produced was low (0.5 to 1.2 m^2/g). We believe that the ambient humidity affected the agglomeration of γ-Al_2O_3 and Li_2CO_3 during physical mixing; and this, in turn, affected the surface area of γ-$LiAlO_2$ obtained after heat treatment, probably because of inhomogenity of the reactant mixture.

During this quarter, three samples of γ-$LiAlO_2$ were synthesized from a low-cost $Al(OH)_3$* and Li_2CO_3 by heat treatment at 975, 1075, and 1175 K for 18 h at each temperature. The products were characterized by x-ray diffraction (XRD), scanning electron microscopy (SEM), and surface area measurements. The results of this study are summarized in Table 2. At 975 K, α-$LiAlO_2$ was obtained as clump-shaped particles of low surface area, 9.3 m^2/g. At higher temperatures (1075 and 1175 K), the surface area of the γ-$LiAlO_2$ was even lower, in fact too low for suitable application of this material in electrolyte structures. At this time, heat treatment of physical mixtures of Li_2CO_3 and $Al(OH)_3$ does not appear promising for synthesizing γ-$LiAlO_2$ for use in electrolyte structures.

---

*Type H-705 $Al(OH)_3$ obtained from the Aluminum Company of America (ALCOA).

Table 1. Synthesis of γ-$LiAlO_2$ for Sintered Tile Structures (starting material: Degussa γ-Al_2O_3 and stoichiometric Li_2CO_3)

Sample No.	Preparation Date in 1979 (Month-Day)	Relative Humidity, %	Room Temp., °F	Heat Treatment: Time at 875 K, h	Heat Treatment: Time at 1175 K, h	$LiAlO_2$ Surface Area, m^2/g
134-63[a]	1-17	10	69	66	16	7.5
134-67[a]	2-12	8	70	82	20	6.0
134-76[a]	3-27	10	74	18	16	7.6
134-79[a]	5-14	20-25	84	65	16	2.5
134-82[b]	5-21	20	79	18	16	0.4
134-83[b]	5-22	20	79	18	16	0.4
134-93-1[a]	6-13	45	82	80	16	1.2
134-93-2[a]	6-13	45	82	40	16	0.6
134-96[a]	7-9	40-50	81	27	16[c]	0.5
134-98[a]	7-11	40-45	84	24	16[d]	0.6

[a]Mixed in jar containing two alumina balls (1.25-cm dia).

[b]Mixed in jar containing two rubber stoppers (#10).

[c]Time at 1225 K.

[d]Time at 1155 K.

Table 2. Synthesis of $LiAlO_2$ from Physical Mixtures of Li_2CO_3 and $Al(OH)_3$

Sample No.	Heat Treatment Temperature[a], K	Physical Characteristics of $LiAlO_2$		
		$LiAlO_2$ Phase	Surface Area, m^2/g	Particle Shape
134-101	975	α	9.3	Clumps
134-103	1075	γ α (mi.)	1.2	Fused Clumps
134-102	1175	γ	0.6	Bipyramids

[a]A heat treatment of 18 h.

Previous experiments indicated that high-surface-area β-$LiAlO_2$ was obtained when Degussa γ-Al_2O_3 (ANL-77-29, p. 11) or Type H-705 $Al(OH)_3$ (ANL-78-71, pp. 4-6) was impregnated with an aqueous solution of LiOH, dried at 425 K, and reacted at 725 K for 1.5 h. Eight samples were prepared to evaluate this type of $LiAlO_2$ in sintered structures. As shown in Table 3, with the exception of two samples (159-134 and 56-60A), each sample was prepared by dissolving LiOH in H_2O, adding $Al(OH)_3$ or Al_2O_3 to the LiOH solution, and then mixing with a magnetic stirrer. In samples 159-134 and 56-60A, the Al_2O_3 was first suspended in H_2O, then the LiOH solution was added to the suspension, which was mixed with a magnetic stirrer. The latter technique is believed to produce better reactant mixing. In some of the samples, a gel formed when all of the reactants were added, thereby stalling the stirrer; these samples are identified in Table 3. The slurries (or gels) were dried at ~425 K, then reacted at ~725 K for 1.5 h. Results of surface area and x-ray diffraction analyses are also reported in Table 3.

Each of the β-$LiAlO_2$ samples was pressed into a pellet and then sintered. As shown in Table 4, the porosities of the sintered pellets prepared from the Type C-33 $Al(OH)_3$ were high (~60%). For the sintered pellets prepared from Degussa γ-Al_2O_3 or Type H-705 $Al(OH)_3$, the porosity was low (30 to 35%) if a gel had formed during mixing of the reactants; when this gel had not formed, the porosity of the sintered pellet was high (60%). Some of the β-$LiAlO_2$ from sample 159-109b, which had formed a gel during preparation, was washed with acetic acid/acetic anhydride followed by methanol to remove the LiOH and/or Li_2CO_3; subsequently, the porosity of the washed β-$LiAlO_2$ sample (159-124) was not affected by the sintering operation. Thus, the LiOH and/or Li_2CO_3 were responsible for the decreased porosity after sintering due to inadequate reactant mixing. Mixtures used to prepare $LiAlO_2$ must be mixed thoroughly prior to sintering.

Table 3. Preparation of β-$LiAlO_2$ by Impregnation Technique (stoichiometric amounts of LiOH and $Al(OH)_3$ or Al_2O_3 were used)

Sample No.	Type of Alumina	Moles $LiAlO_2$[a]	Volume H_2O, L	X-ray Analyses	Surface Area, m^2/g	Gel Formed
134-117	Type C-33[b] $Al(OH)_3$	0.68	0.25	β-$LiAlO_2$ γ-Al_2O_3 (mi.)	40	No
134-120	Type C-33[b] $Al(OH)_3$	2.06	0.75	β-$LiAlO_2$ γ-Al_2O_3 (mi.)	42	No
134-105	Type H-705[b] $Al(OH)_3$	1.36	1.00	β-$LiAlO_2$ γ-Al_2O_3 (mi.)	13	Yes
134-110	Type H-705[b] $Al(OH)_3$	1.36	0.50	β-$LiAlO_2$ γ-Al_2O_3 (v. mi.)	18	Yes
159-109b	Degussa γ-Al_2O_3	1.34	0.70	β-$LiAlO_2$ Li_2CO_3 (mi.) γ-Al_2O_3 (v. mi.)	34	Yes
56-60A	Degussa γ-Al_2O_3	0.76	0.60	β-$LiAlO_2$	47	No
159-134	Degussa γ-Al_2O_3	1.34	1.06	β-$LiAlO_2$ Li_2CO_3 (med.) γ-Al_2O_3 (med.)	32	No
159-124	159-109b washed[c]	-	-	β-$LiAlO_2$ γ-Al_2O_3 (mi.)	-	-

[a] Amount of $LiAlO_2$ expected based on complete reaction of LiOH and Al_2O_3 or $Al(OH)_3$.

[b] Obtained from ALCOA.

[c] Sample was washed with acetic acid/acetic anhydride, then with methanol.

Table 4. Results of Sintering β-$LiAlO_2$ Prepared by Impregnation Technique

Pellet No.	Sample No.	Sintering Temperature, K	Sintering Time, h	Cold-Pressed Porosity, %	Sintered Porosity, %
P-159-132-4	134-117	1265	0.5	60.0	61.7
P-159-128-3	134-120	875 1265	23	61.3	62.7
P-126-1	134-120	875 1265	3 0.75	60.1	61.1
105-1	134-105	1400	1	61.1	32.5
110-1	134-110	1175	3	58.3	30.4
P-159-128-1	134-110	875 1265	3 0.75	56.5	20.1
P-159-128-2	159-109b	875 1265	23 0.1	53.1	31.2
P-126-2	159-109b	875 1265	3 0.75	53.8	31.8
159-109b	159-109b	1265	1.0	52.1	34.5
P-159-132-1	56-60A	1265	0.5	61.9	67.2
P-159-135-1	159-134	1265	0.5	62.7	63.9
P-126-3	159-124	875 1265	23 0.1	55.1	55.1
159-124	159-124	1265	1.0	54.3	53.9

III. DEVELOPMENT OF SINTERED LITHIUM ALUMINATE STRUCTURES

(R. N. Singh, J. T. Dusek, R. E. Mailhiot, and R. B. Poeppel)*

Ceramic processing techniques are being explored to produce stable lithium aluminate structures of controlled microstructure (porosity and pore size). During this quarter, γ-$LiAlO_2$ pellets in the shape of small discs and plates ($\sim$12.5 x 12.5 x 0.15 cm), with and without wire reinforcement, were sintered.

A summary of powder characteristics, sintering conditions, and sintered porosities is given in Table 5. This table also contains results for two sintered samples prepared from α-$LiAlO_2$ (in these cases, the α-to-γ transition occurred during sintering). Differences in starting materials led to a rather wide range of final porosities, as shown in Table 5; many samples had porosities well below the desired 60%. Porosities of 60% were obtained by sintering α and γ powders from batch numbers 134-60 and 134-63, respectively; however, under similar specimen preparation conditions, the porosities of the sintered structures obtained from more recent batches of γ-$LiAlO_2$ powder (batch numbers 134-67, -76, -79, -82, and -83) have been consistently low ($\sim$45% porosity). As discussed in Section II, one of the reasons for this may be the relatively low surface area of the recent γ-$LiAlO_2$ powders (see Table 1).

A sintered sample from each batch was examined by SEM. Microstructures for the high-porosity samples prepared from batches 134-63 and 134-60, which are presented as Figs. 1 and 2, respectively, show uniformly small particles. In contrast, microstructures typical of low-porosity samples prepared from batches 134-67, -76, and -79, shown in Fig. 3, consist of a large fraction of relatively large agglomerates. Although batch 134-67 contained some fine particles, the fraction of fine particles was progressively smaller in batches 134-76 and -79. Low-porosity samples were also prepared from batches 134-82 and -83; the SEM's for these batches showed particles that were uniformly large (Fig. 4). These findings suggest that high-porosity sintered structures are obtained from $LiAlO_2$ powders of small particle size and/or high surface area.

In the two-step heat-treatment used to prepare the γ-$LiAlO_2$ powders (see Section II), the first treatment at 875 K produced α-$LiAlO_2$, and the second treatment at 1175 K converted the α- to γ-$LiAlO_2$. The particle growth occurred during the second step; and, therefore, α-$LiAlO_2$ samples were maintained at temperatures of 973, 1023, and 1073 K to determine whether this conversion step might be performed at a lower temperature. The results (Table 6) indicate that the minimum temperature for the transformation occurs between 973 and 1023 K.

The γ-$LiAlO_2$ powder prepared by heat treating α-$LiAlO_2$ (batch 134-99) at 1073 K for 50 h was cold pressed into three discs (32-mm dia x 2.5-mm high) and then sintered at 1383 K for 2 h. In addition, γ-$LiAlO_2$ prepared by maintaining the α-$LiAlO_2$ at 1023 K for 50 h was cold pressed into a disc and sintered at 1273 K for 2 h. Table 7 shows that the porosity of these sintered samples ranged from 47-58%. Thus, the lower transformation

---

*Materials Science Division, ANL

Table 5. Porosity of Sintered $LiAlO_2$ Structures

Sample Number	Powder Batch Number[a]	Powder Surface Area, m^2/g	Powder Preparation	Sintering Temp., K	Sintering Time, h	Porosity, %
40	134-67 (γ)	6	Ball milled[b]	1373	0.5	52.6
63	134-67 (γ)	6	Ball milled	1373	4	53.0
65	134-76 (γ)	7.6	Ball milled	1373	4	44.1
67	134-79 (γ)	2.5	Ball milled	1373	4	44.7
69	134-82 (γ)	0.35	Ball milled	1373	4	45.2
71	134-83 (γ)	0.44	Ball milled	1373	4	45.5
38	134-60 (α)	69	None	1373	0.5	59.3
58	134-60 (α)	69	None	1473	2	36.7
2-P	134-63 (γ)	7.5	None	1373	0.5	60.0
3-P	134-63 (γ)	7.5	None	1373	0.5	61.4
78	134-79 (γ)	2.5	Ball milled with 15 wt % corn starch and ethanol	1373	3.5	56
93	Mix[c]	-	Ball milled with 15 wt % corn starch and ethanol	1373	2	54
11-P	Mix[d]	-	Ball milled with 15 wt % corn starch and ethanol	1373	2	55

[a] The $LiAlO_2$ phase is indicated within parentheses.

[b] Ball milled for ~20 h in ethanol.

[c] Four grams each from batches 134-76, -79, -82, -83, -93-1, and -93-2.

[d] One hundred grams each from batches 134-76, -79, -82, -83, and -93-2; 67 grams from batch 134-93-1

Fig. 1. Microstructure of Sintered γ-$LiAlO_2$ from Batch 134-63 Containing Uniformly Small Particles. (Magnification, 12,000X.)

temperatures (1023 and 1073 K) resulted in an improvement in porosity over the ∿45% porosities of sintered samples prepared from earlier batches of powder (transformation temp., 1175 K). However, SEM examination of these four sintered samples revealed the presence of undesirably large particles. Even the sample prepared at 1023 K (Sample 115 in Table 7) resulted in a sinter with large particles. To determine at what point these large particles were formed, samples were cold pressed from the α-$LiAlO_2$ of batch 134-99 and from γ-$LiAlO_2$ produced from this α-$LiAlO_2$ heat treated at 1073 K; SEM examination of these samples revealed large particles only in the γ powder samples.

Attempts also were made to modify the existing powder through the incorporation of additives (as binders) which would burn off during the sintering operation and leave a structure of high porosity. As indicated in Table 5, sample 78 had ∿15 wt % corn starch added to γ-$LiAlO_2$ (batch 134-79); after sintering, this sample had a ∿10% higher porosity than that of a similar sample without the additive (sample 67). Because of this initial success, a ∿12.5-cm square plate was prepared by mixing several batches of the low-surface-area powders with corn starch, cold pressing, and sintering; this procedure resulted in a plate (11-P) with a porosity of ∿55%. This sample, which is reinforced with Kanthal wire, will be impregnated with the electrolyte mixture and, if found to be crack free, will be tested in 10-cm square

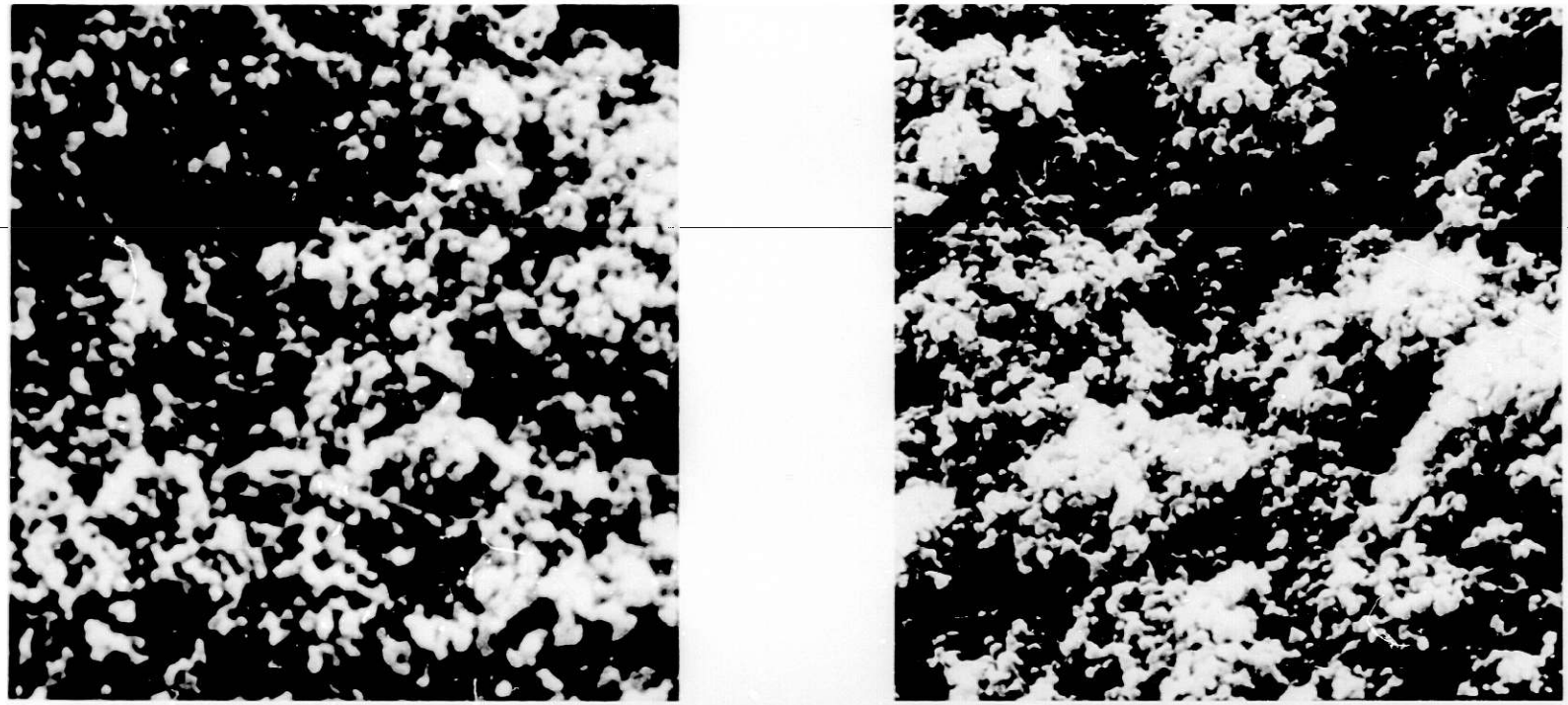

(a) (b)

Fig. 2. Microstructure of Sintered α-$LiAlO_2$ from Batch 134-60 Containing Uniformly Small Particles. (Magnification 12,000X.)

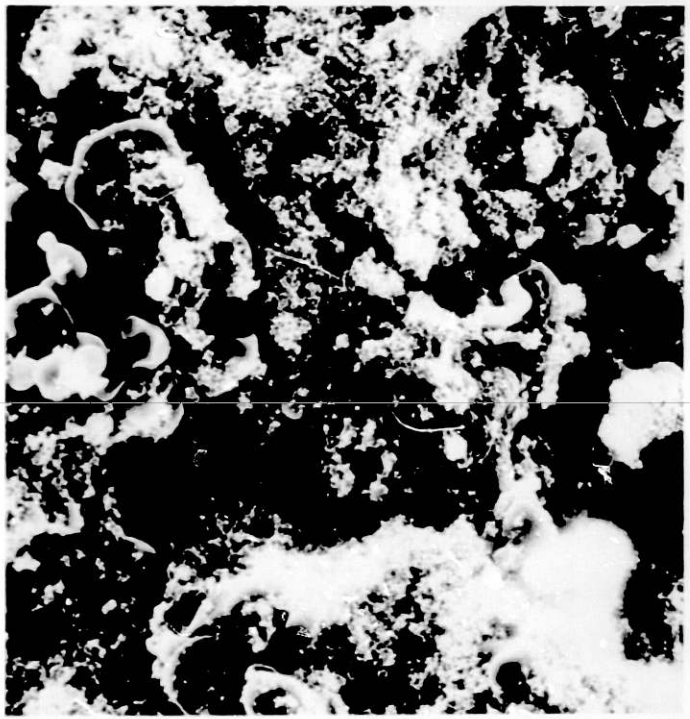

Fig. 3. Microstructure Typical of Sintered $LiAlO_2$ Prepared from Batches 134-67, -76, and -79 Containing Large Agglomerates. (Magnification, 1500X.)

Fig. 4. Microstructure Typical of Sintered $LiAlO_2$ Prepared from Batches 134-82 and -83 Containing Uniformly Large Particles. (Magnification, 1500X.)

Table 6. Heat Treatment of α-$LiAlO_2$ Powder

Powder Batch No.	Allotropic Form	Heat Treatment Conditions		X-ray Analysis After Heat Treatment[a]
		Temp., K	Time, h	
134-99	α-$LiAlO_2$	1073	24	γ, α (v.v. minor)
		1073	50	γ, α (v. minor)
		1023	24	γ, α (v. minor)
		1023	50	γ, α (v. minor)
		973	24	α, γ (minor)
		973	50	α, γ (minor)

[a] A major phase unless otherwise indicated.

cell housings. An additional sample without wire reinforcement has been cold pressed and will be sintered in the near future.

Because of our recent difficulties in producing high-porosity, sintered structures utilizing γ-$LiAlO_2$ powders, attempts were made to fabricate plates directly from α-$LiAlO_2$ powder. Initial experiments demonstrated that samples in the form of plates ($\sim$13-cm square) with porosities as high as 64% can be fabricated from the α-$LiAlO_2$ powder. The use of a die lubricant prevented the α-$LiAlO_2$ from sticking to the die during cold pressing. The sintered plates contained local depressions, which are probably areas of increased density caused by the presence of unreacted Li_2CO_3 in the starting powder. Attempts are now being made to eliminate unreacted Li_2CO_3 from the α-$LiAlO_2$ powder either by sieving (Li_2CO_3 promotes clumps) or by washing the powder with a mixture of acetic acid and acetic anhydride. The presence of unreacted Li_2CO_3 also may have been responsible for the low surface area of γ-$LiAlO_2$ powders, which have consistently produced low-porosity samples in recent months. Attempts are being made to produce α-$LiAlO_2$ powders with as little unreacted Li_2CO_3 as possible by controlling the ratio of γ-Al_2O_3 to Li_2CO_3, and by better mixing of the starting powders.

Table 7. Results of Sintering γ-$LiAlO_2$ Pressed Samples (batch 134-99)

Sample No.	Pressing Load, kg	Green Porosity, %	Sintering Conditions		Sintered Porosity, %	SEM Observation
			Temp., K	Time, h		
103[a]	455	-	1383	2	53	Large agglomerates
104[a]	455	-	1383	2	52	-
105[a]	136	-	1383	2	58	Large agglomerates
106[a]	136	56	-	-	-	Large agglomerates
115[b]	455	-	1273	2	47	Large agglomerates

[a] α-$LiAlO_2$ powder (batch 134-99) transformed to γ-$LiAlO_2$ at 1073 K for 50 h.

[b] α-$LiAlO_2$ powder (batch 134-99) transformed to γ-$LiAlO_2$ at 1023 K for 50 h.

IV. EVALUATIONS OF ELECTROLYTE STRUCTURES

(R. N. Singh, D. S. Kupperman, N. P. Lapinski,
R. E. Mailhiot, and R. B. Poeppel)*

A reinforced sintered structure (6-P) that had been tested in a circular cell (see Section VI) was examined by x-ray radiography. After disassembly of the cell, a crack emanating from one edge of the sample was seen (Fig. 5). This crack did not appear to propagate into the center of the sample through the wet-seal area. Posttest examination by SEM is under way to characterize the sintered structure after cell testing.

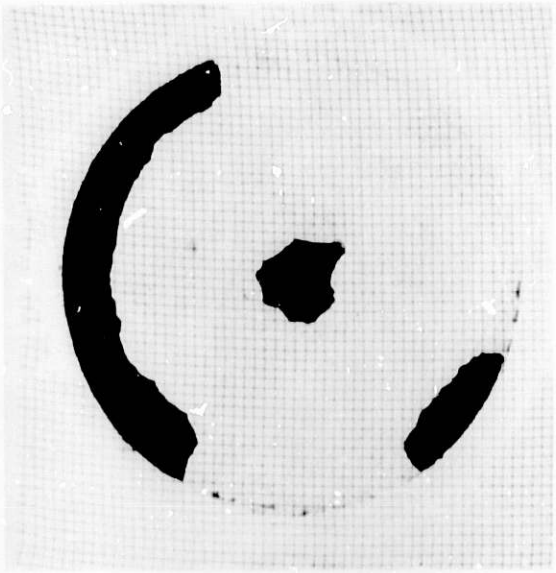

Fig. 5. X-ray Radiograph of Sinter 2 after Cell Testing Showing a Crack Emanating from One Edge

An earlier sintered specimen (not reinforced) which had been tested in cell Sinter 1 (ANL-79-84, p. 30) was sampled in two locations outside and inside the cell housings. These samples were then examined by SEM. The sample obtained from inside the cell housings appeared to have lost some electrolyte at the cracked surface (Fig. 6a), whereas the sample obtained from outside the wet seal appeared to be completely impregnated by the electrolyte mixture (Fig. 6b). The photo-micrograph shown in Fig. 6b is typical of an impregnated sintered structure as shown in Fig. 7. This finding suggests increased loss of electrolyte from the cracked surface in the presence of cross leakage of reactant gases over the electrolyte loss to static air outside the cell. More samples are being examined to determine if this is a general phenomenon.

---

*Materials Science Division, ANL

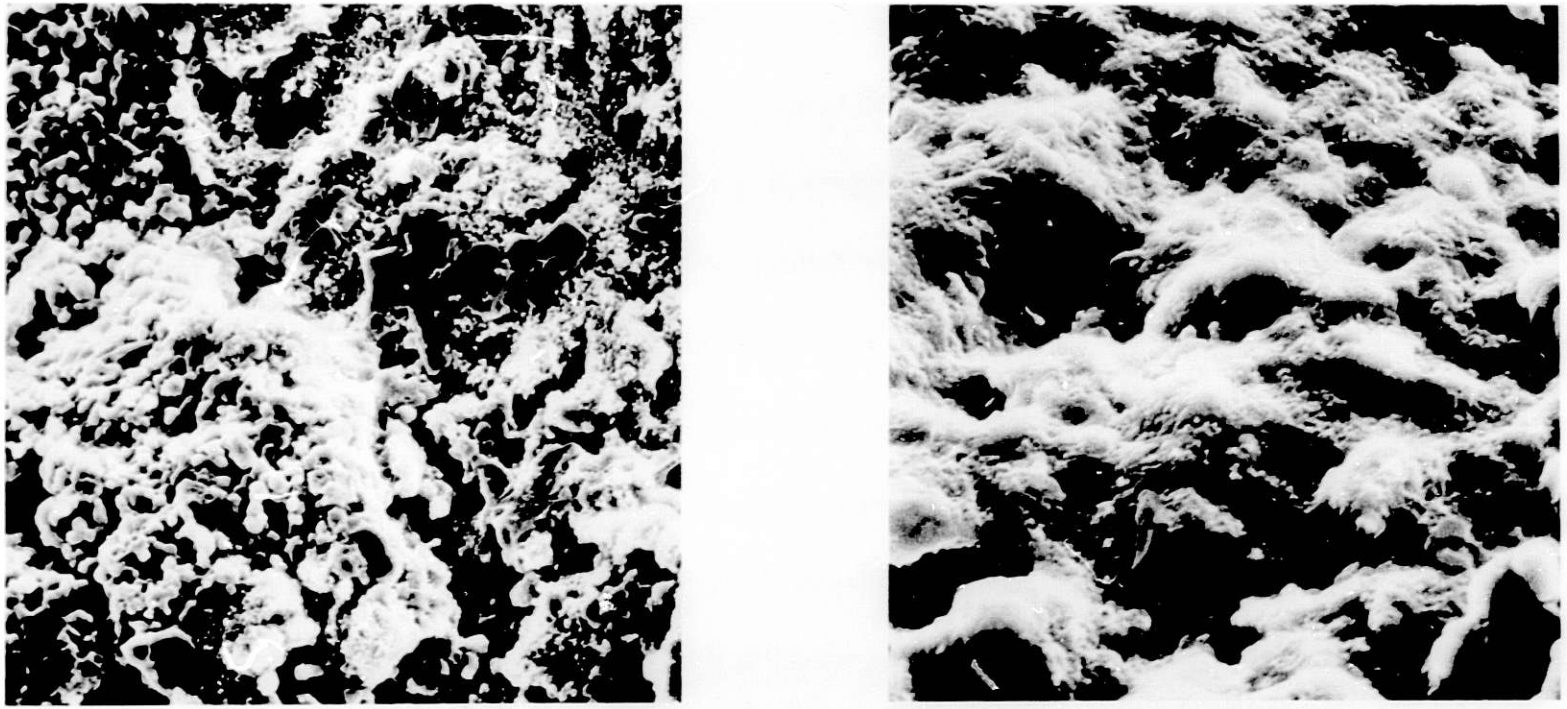

(a) (b)

Fig. 6. Scanning-Electron Micrograph of Sinter 1 after Cell Testing. (a) Surface of a Crack in an Area Inside the Cell Housing (Magnification, 1000X). (b) Surface of a Crack in an Area Outside the Cell Housing (Magnification, 2200X).

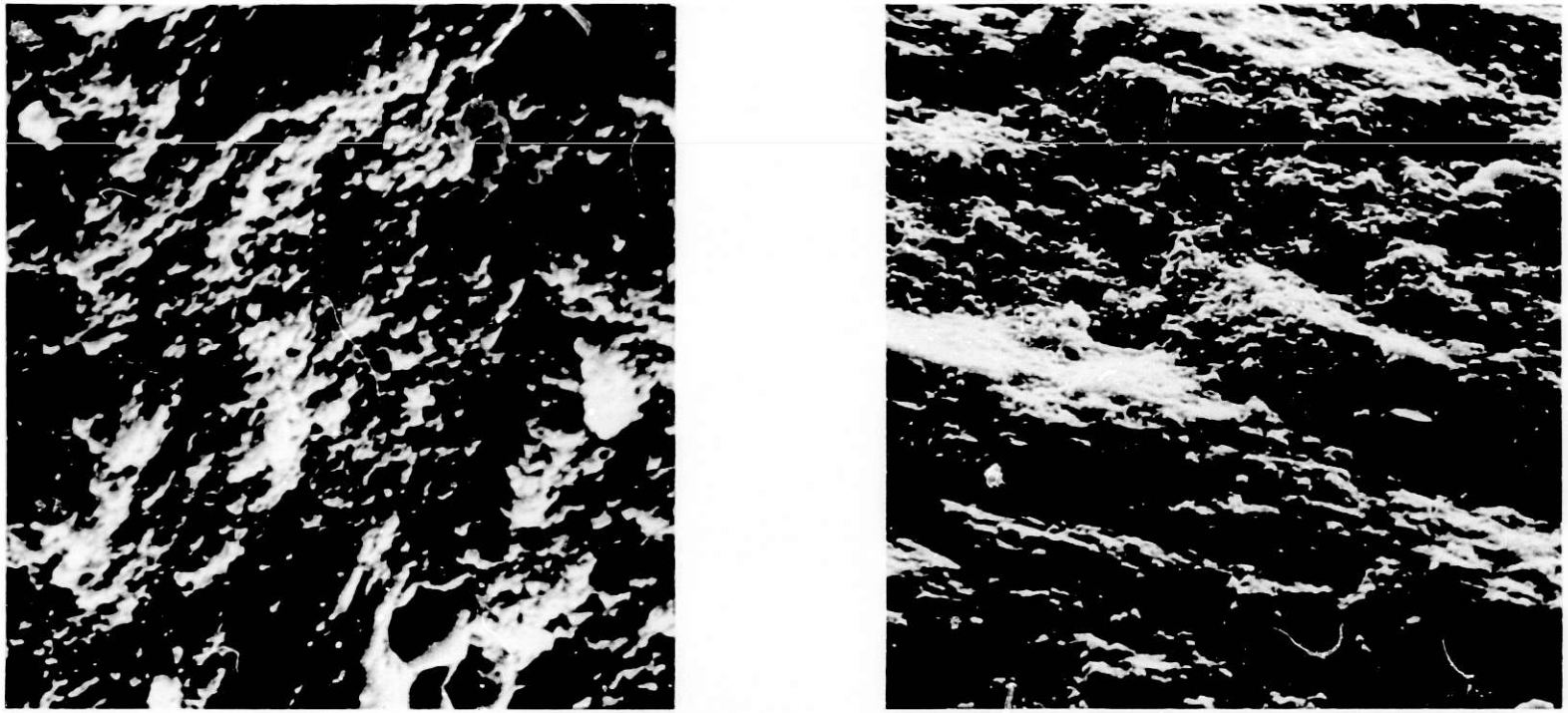

(a) (b)

Fig. 7. Micrograph of Sintered Structure Completely Impregnated by Electrolyte. (a) Magnification, 440X. (b) Magnification, 4800X.

As reported in the previous quarterly (ANL-79-84, p. 33), a hot-pressed tile tested in a 10-cm square cell (cell SQ-7) was examined, and areas that appeared quite inhomogeneous with respect to the distribution of γ-$LiAlO_2$ and electrolyte mixture were found. Since then, a hot-pressed tile (T159-57) was examined to determine whether this inhomogeneous structure was generated during tile synthesis or subsequent cell testing. Figure 8 shows an SEM of tile T159-57; this microstructure appears inhomogeneous, with evidence of areas that are rich in γ-$LiAlO_2$ (lighter areas) and electrolyte mixture (darker areas). There also appears to be a gap between the Kanthal wire and the ceramic microstructure (see Fig. 8a). Therefore, the inhomogenity is present in the as-fabricated tiles. Attempts will now be made to change the tile preparation techniques to produce a more homogeneous microstructure.

In addition, one 13-cm-square sintered plate (11-P) and five hot-pressed tiles (158-89, -95, -96, -101, -103) were examined by x-ray radiography. The sintered structure (11-P) showed no cracks. Three of the hot-pressed tiles (159-89, -95, and -103) contained cracks. Tile 159-96 had broken reinforcement Kanthal wire but no apparent cracks, and Tiles 159-101 and -95 showed evidence of low-density areas.

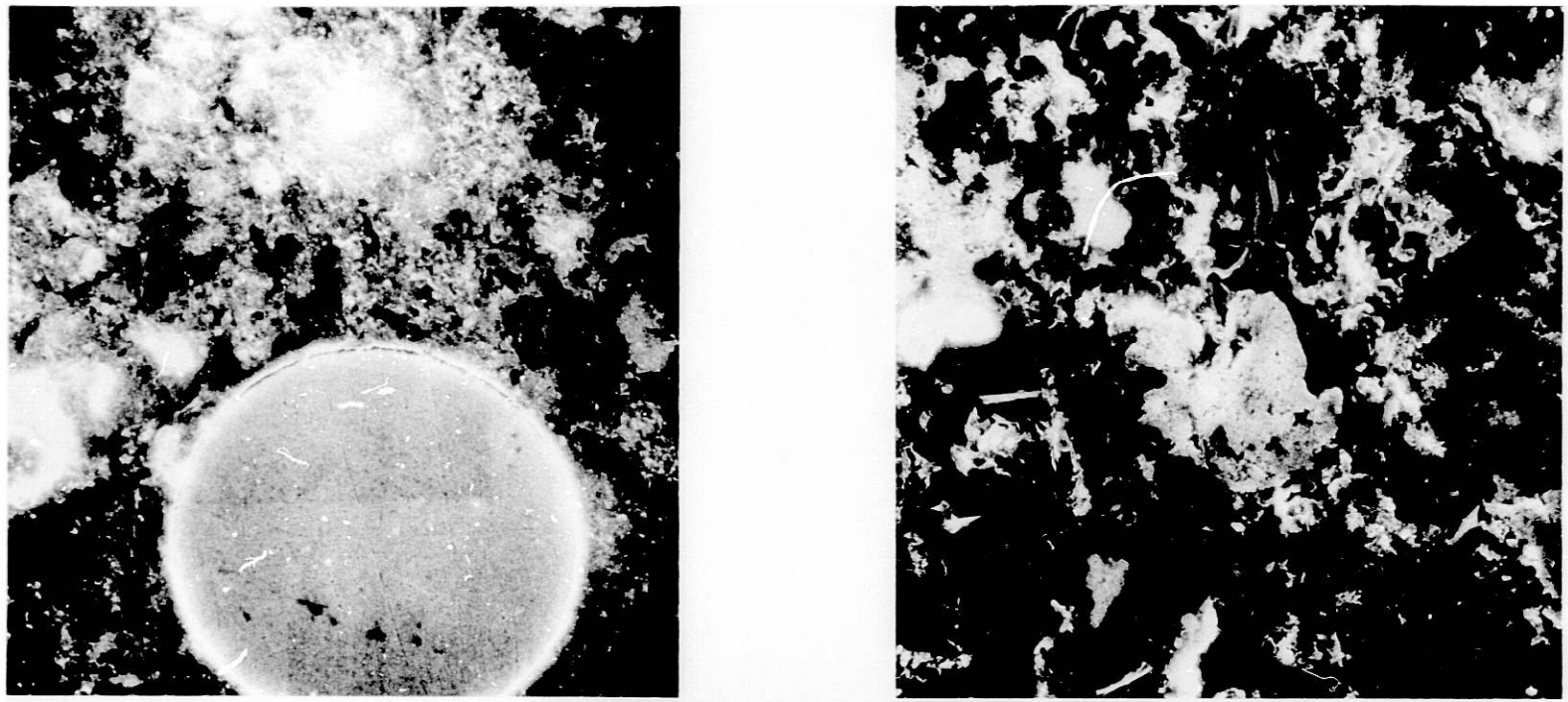

(a) (b)

Fig. 8. Microstructure of Tile T159-57 As-Fabricated.
(a) Magnification, 480X.
(b) Magnification, 1000X.

V. THERMOMECHANICAL TESTING OF ELECTROLYTE STRUCTURES
(G. H. Kucera)

The effect of electrolyte content on the coefficient of linear thermal expansion and creep behavior has been determined for six hot-pressed pellets containing high-surface-area (26 m^2/g) γ-$LiAlO_2$ and variable amounts (6.4 to 84.2 vol %) of Li_2CO_3-K_2CO_3 eutectic. For this series of experiments, the thermal expansion was measured with a dilatometer (ANL-79-84, p. 27) for six hot-pressed pellets. Three of the pellets had ≤55 vol % eutectic and the thermal measurement conditions were as follows: a compressive stress of 98.6 kPa, a CO_2 environment, a thermal cycle of room temperature to ∿725 K. For the three other pellets with ≥58 vol % eutectic, the measurement conditions were the same except that the temperature range was decreased to ∿650 K because at ∿675 K such structures tend to compress slightly under the minimum applied load in our dilatometer. Table 8 presents the measured coefficient of linear thermal expansion for the six hot-pressed pellets. Each value given is the average of about ten measurements.

Table 8. Coefficient of Linear Thermal Expansion for γ-$LiAlO_2$ (26 m^2/g) and Variable Amounts of Li_2CO_3-K_2CO_3 Eutectic

Volume % Li_2CO_3-K_2CO_3[a]	α, per °C x 10^{-6}
6.4	12.0 ± 1.8[b]
17.4	12.4 ± 2.9[b]
36.1	17.4 ± 2.5[b]
58.9	25.8 ± 2.8[c]
72.6	27.2 ± 0.6[c]
84.2	30.6 ± 1.5[c]

[a] At room temperature, based on a solid density for Li_2CO_3-K_2CO_3 of 2.27 g/cm^3.

[b] Temperature range of 300 to 725 K.

[c] Temperature range of 300 to 650 K.

For a composite structure, such as $LiAlO_2$ plus Li_2CO_3-K_2CO_3, the coefficient of thermal expansion (α) might be expected to follow the simple rule of mixtures:

$$\alpha_{mix} = \sum^{n} \alpha_n Z_n \qquad (1)$$

where α_n is the coefficient of thermal expansion of phase n, and Z_n is the volume fraction of phase n. However, Turner[1] has suggested that a state of stress exists between the phases which influences the thermal expansion behavior of the composite structure. Turner expresses the coefficient of

thermal expansion as:

$$\alpha_{mix} = \sum^{n} \frac{\alpha_n Z_n K_n}{Z_n K_n} \qquad (2)$$

where K_n is the bulk moduli of phase n. A family of curves was generated using Turner's equation, with α_1 of 12.4 x 10^{-6}/°C,[2] α_2 of 33 x 10^{-6}/°C,* and various ratios of K_1/K_2. Figure 9 is a plot of the coefficient of linear expansion as a function of carbonate content for the thermomechanical data in Table 8 as well as previous data (ANL-79-84, p. 28) obtained from samples having γ-$LiAlO_2$ with a surface area of 14 m^2/g; also shown in this figure are the curves obtained from Eqs. 1 and 2. For the latter equation, it was assumed that the K_1 for $LiAlO_2$ is 1.5 times the K_2 for the eutectic. This ratio is consistent with the work by Fahmy and Ragai[4] who have shown that materials with low expansion coefficients generally have high bulk moduli. The data from the two sets of experiments are in good agreement, within experimental error, and appear to fit the Turner equation.

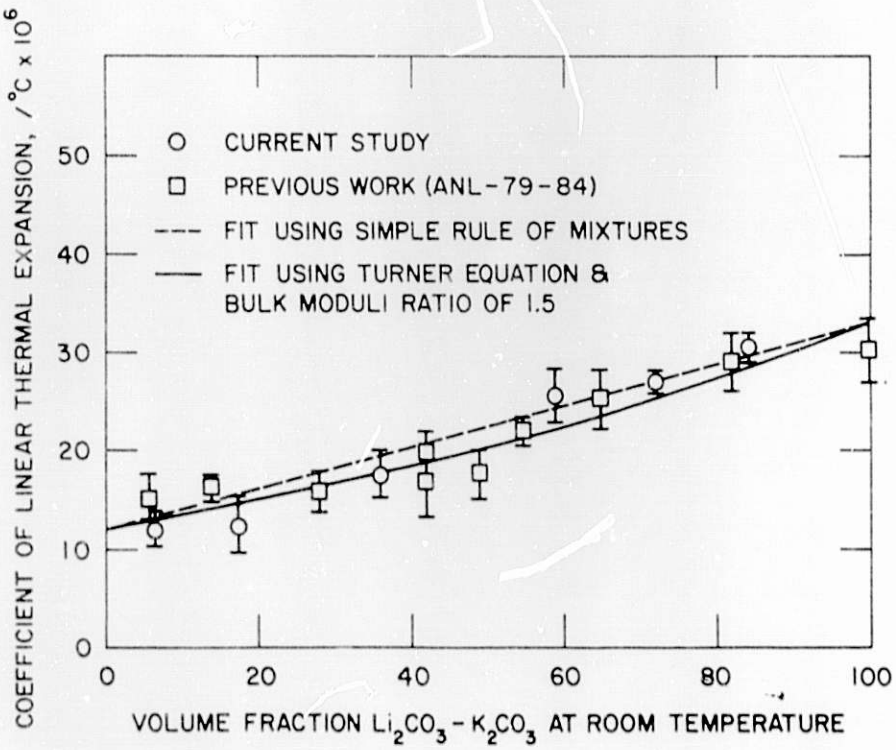

Fig. 9. Coefficient of Linear Thermal Expansion of γ-$LiAlO_2/Li_2CO_3$-K_2CO_3 Mixtures (Room Temperature to 650 K)

*Average obtained from measurements given in ANL-79-84, p. 28 and Ref. 3.

The long-term creep data (100-200 h at 925 K under a compressive stress of 98.6 kPa) for three of the pellets containing <60 vol % eutectic are given in Table 9. As indicated by this table, the greatest primary creep occurs in the first ten hours. This behavior was noted previously (ANL-79-84, p. 28) for structures containing low-surface-area γ-$LiAlO_2$ and varying amounts of eutectic. These data also include the total creep, *i.e.*, the sudden thickness change at the melting temperature of the eutectic (~675 K) plus the primary creep. As shown, the pellet with an eutectic content of 58.9 vol % has a compression of only about 2% at the eutectic melting temperature. In the previous study with low-surface-area γ-$LiAlO_2$, a pellet containing 54.5 vol % eutectic underwent a 5.5% compression at eutectic melting.

Table 9. Creep Behavior of γ-$LiAlO_2$ (26 m^2/g) and Varying Amounts of Li_2CO_3-K_2CO_3

Li_2CO_3-K_2CO_3,[a] vol %	Time, h	Primary Creep at 925 K,[b] % Thickness Decrease	Total Creep, % Thickness Decrease
6.4	10	0.27	0.44
	20	0.27	
	30	0.29	
	100	0.29	
17.4	10	0.6	1.7
	20	0.7	
	100	0.7	
58.9	10	0.4	2.5
	20	0.4	
	30	0.5	
	93	0.5	

[a] Based on a density for (solid) Li_2CO_3-K_2CO_3 of 2.27 g/cm^3 at room temperature.

[b] Compressive load of 98.6 kPa.

VI. CELL TESTING
(J. W. Sim)

In the previous report (ANL-79-84, p. 30), testing of sintered electrolyte structures was initiated in two circular (7-cm dia) cells--Sinter 1 and 2. During this report period, the testing of sintered electrolyte structures was continued with another circular cell, Sinter 3. Even though the circular cell was inferior to the square one, principally because of poor support of the electrodes (ANL-78-40, p. 30), it had to be used for the present cell tests owing to the small size of the available sinters. The characteristics of the components in cells Sinter 1, 2, and 3 are given in Table 10. The non-reinforced structure used for cell Sinter 1 was determined to have had four cracks prior to cell assembly; during operation, this cell exhibited cross-leakage of oxidant into the anode gas stream and failed after two thermal cycles. The failure was apparently caused by one of the hairline cracks present before testing, which enlarged during cell operation.

Cross-leakage did not occur* in cell Sinter 2, which utilized a reinforced, sintered $LiAlO_2$ structure containing no detectable cracks under radiographic examination prior to cell testing. Cell Sinter 2 sustained five thermal cycles without cross-leakage at a differential pressure of 6.9 kPa (1 psi). It was voluntarily terminated to determine the condition of the electrolyte component. The only cracks observed during posttest examination apparently were caused by disassembly of the cell. Both of the cell housings and the electrodes adhered tenaciously to the sintered structure.

Cell Sinter 3 used a reinforced, sintered $LiAlO_2$ structure containing two small ($\sim$0.01 mm wide and $\sim$2-4 mm long) hairline cracks. The purpose of this test was to determine whether the small cracks would result in cross-leakage during cell operation. A low level of cross-leakage was detected before the first thermal cycle (Fig. 10), and an increase was detected after the first thermal cycle (Fig. 11). The level of cross-leakage remained stable through the second thermal cycle (Fig. 11), but the test was terminated because of carbon deposition in the anode inlet tube. In contrast, cross-leakage for cell Sinter 1 also is shown in Figs. 10 and 11. The higher leakage for this cell was to be expected, because the size and number of cracks observed prior to testing were larger for structure 1-P (tested in cell Sinter 1) than for structure 8-P (tested in cell Sinter 3). Both cells showed increased levels of cross-leakage, as shown in Fig. 11. The sintered $LiAlO_2$ structure tested in cell Sinter 3 was apparently more resistant to cross-leakage and to failure than the structure tested in cell Sinter 1. Nevertheless, it appears that cracks detectable by radiographic examination will lead to cross-leakage during cell operation.

We plan to test a non-reinforced, sintered $LiAlO_2$ structure containing no cracks as soon as such a structure can be fabricated to determine whether Kanthal reinforcement helps to prevent the failure of the sintered $LiAlO_2$ electrolyte structure by deterring crack propagation during thermal cycling. Problems with $LiAlO_2$ powder processing have delayed the fabrication of such a structure, however.

---

*See Appendix for cross-leakage measurement technique.

Table 10. Characteristics of Cell Components

	Sinter 1	Sinter 2	Sinter 3
Anode			
Composition	Ni	Ni-10 wt % Cr	Ni-10 wt % Cr
Thickness, mm	0.74	0.74	0.76
Porosity, %	74.2	56.6	64.4
Mean Pore Size, μm	6.8	3.8	4.6
Cathode[a]			
Composition	Ni	Ni	Ni
Thickness, mm	0.64	0.64	0.64
Porosity, %	73.1	74.4	74.4
Mean Pore Size, μm	10.2	9.6	9.6
Electrolyte Structure			
Sinter No.[c]	1-P	6-P[b]	8-P[b]
Thickness, mm	2.5-2.7	1.7-1.8	1.5-1.9
Porosity, %	57	52	53
Radiographic Exam.[d]	Four cracks (∿0.06 x 15 mm, ∿0.06 x 10 mm, ∿0.03 x 10 mm, ∿0.03 x 10 mm)	No cracks	Two cracks (∿0.01 x 4 mm, ∿0.01 x 2 mm)

[a] Characteristics prior to *in situ* oxidation.

[b] Reinforced with Kanthal screen (20 mesh, 0.127 mm wires, at midplane).

[c] Sinter preparation reported in ANL-79-84, p. 8.

[d] Before impregnation with carbonates.

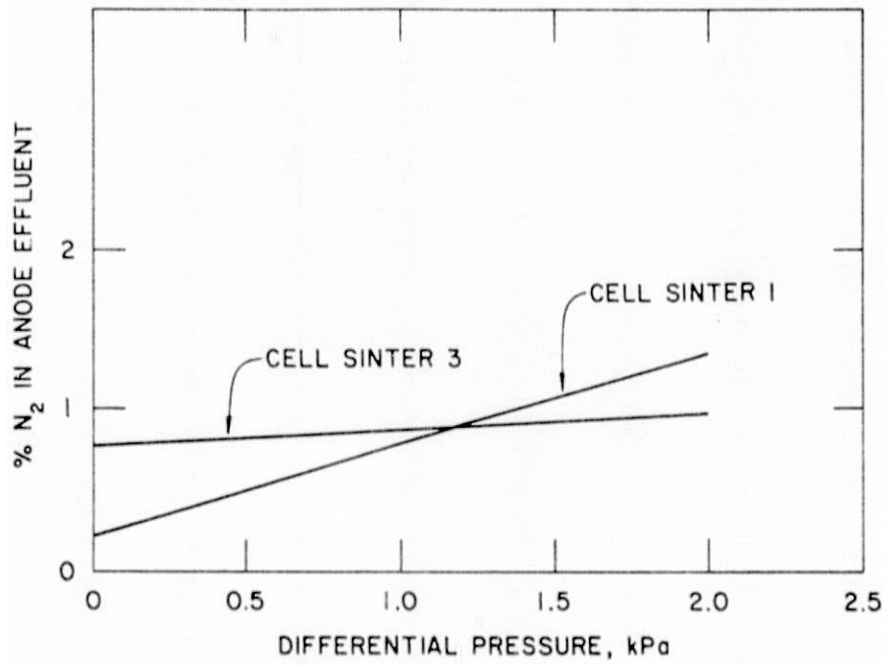

Fig. 10. Cross-leakage in Cells Sinter 1 and Sinter 3 before First Thermal Cycle

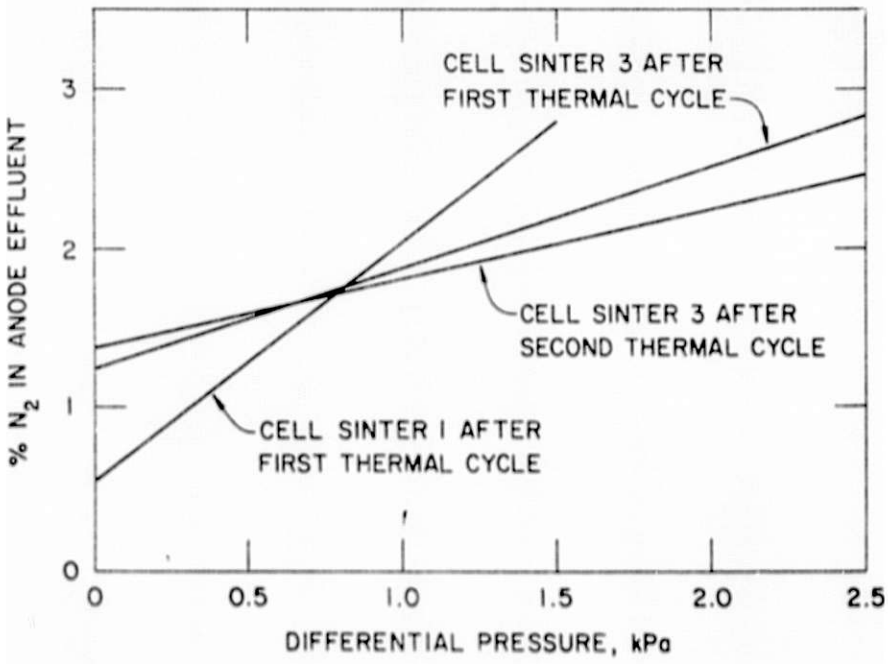

Fig. 11. Cross-leakage in Cells Sinter 1 and Sinter 3 after Thermal Cycling

REFERENCES

1. P. S. Turner, J. Res. Nat. Bur. Std. *37*, 239 (1946).

2. F. A. Hummel, J. Amer. Ceram. Soc. *34*, 235 (1951).

3. Institute of Gas Technology, Report SAN-11276-1, p. 2-63 (Oct. 1979).

4. A. A. Fahmy and A. N. Ragai, *Thermal-Expansion Behavior of Two-Phase Solids*, J. Appl. Phys., Vol. 41, p. 5108 (1970).

APPENDIX

Our test for cross-leakage involves measuring the amount of nitrogen in the anode exhaust while varying the differential pressure between the cathode (above atmospheric pressure) and the anode (at atmospheric pressure). Because the gas entering the anode contains no nitrogen (helium is used during the cross-leakage measurements), while the cathode gas contains 57.5% nitrogen, an increase in measured nitrogen with increased differential pressure indicates cross-leakage of oxidant into the anode gas stream. The nitrogen measured in the anode exhaust with no differential pressure applied is due to diffusion of ambient air past the wet-seal area of the anode. This was established by maintaining a constant differential pressure between the electrodes while increasing the pressure within the anode. Under these conditions, the amount of nitrogen decreased with increasing anode pressure. An example of such a measurement is shown in Fig. 12. Thus, we use the increase in measured nitrogen with increasing differential pressure between the electrodes to quantify cross-leakage.

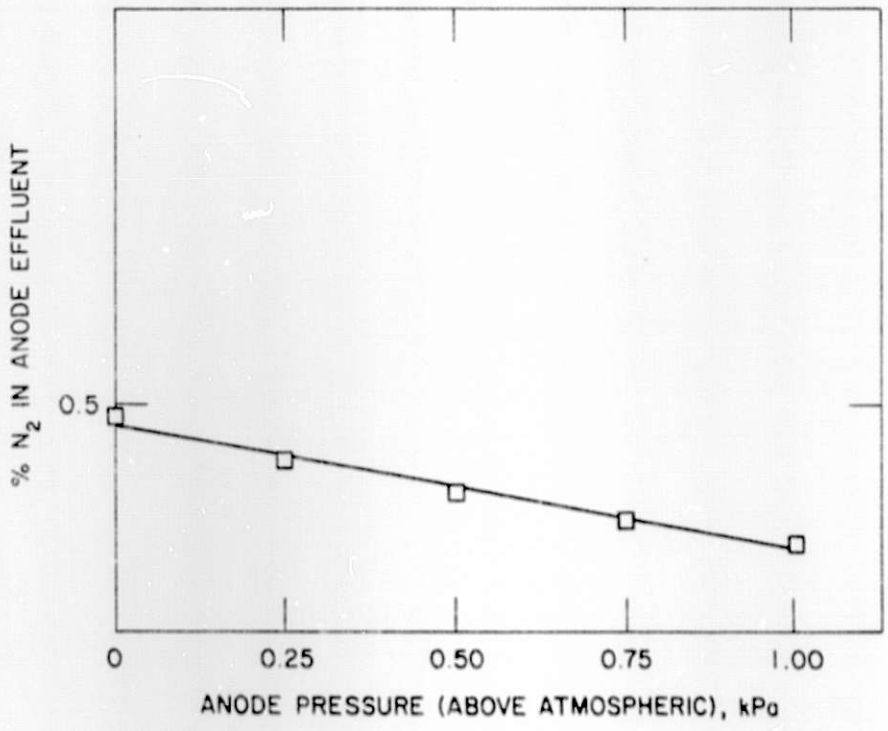

Fig. 12. Decreasing Nitrogen Content in Anode Effluent with Increasing Anode Pressure (differential pressure between cathode and anode is constant at 0.50 kPa)